A three-step, three-gamma model for the numerical modeling of the critical height of the propagation of semi-confined detonation waves

S. Taileb[§], E. Rougon[†], V. Robin[†], V. Rodriguez[†], P. Vidal[†] ,
S. S.-M. Lau-Chapdelaine[‡], J. Melguizo-Gavilanes[†] , A. Chinnayya[†]

[†] Institut PPRIME - UPR 3346 - CNRS - ISAE-ENSMA - Université de Poitiers, France

[‡]Department of Chemistry and Chemical Engineering, Royal Military College of Canada, Kingston, ON, Canada K7K7B4

[§]M2P2, UMR 7340, Aix Marseille University, CNRS, Centrale Marseille, France

1   Introduction

Gaseous detonation waves are supersonic combustion waves, propagation of which depends of its surroundings [1]. When the gaseous mixture is confined by an inert layer, lateral expansion of the products and streamline divergence are responsible of the velocity deficit, as compared to the ideal Chapman-Jouguet velocity, and ultimately can quench the detonation wave. The determination of this critical height is of importance, for propulsion applications, in rotating detonation engines [2] and for safety [3] in industrial and nuclear plants. This canonical configuration has also been heavily studied in the context of explosives (see review of [4]). Reynaud et al. [5,6], Mi et al. [7], Houim and Fievisohn [8] performed numerical simulations using a one-step, one-γ model. The numerical critical heights from Reynaud were not consistent with the experimental results. Taileb et al. [9] and Shigeoka et al. [10] found that the use of detailed chemistry enabled to recover the experimental trends, at least for hydrogen-oxygen at ambient conditions. However, the computational cost required to the use of detailed chemistry remains quite prohibitive. Calibration processes have been proposed by Kaplan and al. [11], where fewer calibration coefficients (isentropic coefficient and heat of reaction) have been used in a one-step global reaction. Houim and Taylor [12] have shown that they could reproduce the shock to detonation transition. Veiga et al. [13] have tried to match the $D - \kappa$ curve. Nevertheless, chemical conversion of reactants does not always take place through a global step, but rather through a sequence of intermediate steps. The three-step model [14–16] enjoys some of these properties, through a sequence consisting of initiation, branching and termination steps. Some of the initial constraints of this model, which were probably initially present for analytic traceability can be loosened, namely different molecular weights and heat capacities. This numerical study reports some of these calibration efforts used to recover the critical height from a three-step, three-γ model, the reference being the one obtained from the detailed chemistry.

2   Mathematical model and numerical methods

The 2-D reactive Euler equations are used for this study. Full details of the high-fidelity numerical schemes and the computational implementation can be found in Reynaud et al. [5, 6], Taileb et al. [9]. A three-step chain branching model is used to model the kinetics of $2\,H_2 + O_2$ at atmospheric pressure and ambient temperature. The chemical decomposition is represented by:

$$\text{Initiation} \qquad \mathcal{F} \longrightarrow \mathcal{Y} \tag{1}$$

$$\text{Branching} \qquad \mathcal{F} + \mathcal{Y} \longrightarrow 2\mathcal{Y} \tag{2}$$

$$\text{Termination} \qquad \mathcal{Y} \longrightarrow \nu \mathcal{P} \tag{3}$$
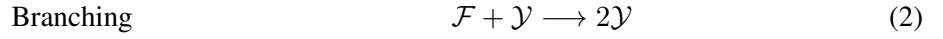
where $\nu = W_{\mathcal{Y}}/W_{\mathcal{P}}$ is the stoichiometric coefficient, which is the ratio of the molecular weights of the intermediate and the products species. The enthalpy reads $h = Y_{\mathcal{F}}h_{\mathcal{F}} + Y_{\mathcal{Y}}h_{\mathcal{Y}} + Y_{\mathcal{P}}h_{\mathcal{P}}$ such as each specific enthalpy is assumed to be a linear function of the temperature $h_k = h_k^0 + c_{p,k}T$. The mixture capacity heat is given by $c_{p,m} = \sum c_{p,k}$ and the molecular weight is $1/W = \sum(Y_k/W_k)$. Only the third step releases heat.

From the ZND model [17], the Master equation for the velocity can be obtained

$$(1 - M^2)\frac{\mathrm{d}u}{\mathrm{d}x} = \left(\frac{W}{W_{\mathcal{F}}} - \frac{c_{p,\mathcal{F}}}{c_{p,m}}\right)\frac{\mathrm{d}Y_{\mathcal{F}}}{\mathrm{d}t} + \left(\frac{W}{W_{\mathcal{Y}}} - \frac{c_{p,\mathcal{Y}}}{c_{p,m}}\right)\frac{\mathrm{d}Y_{\mathcal{Y}}}{\mathrm{d}t} + \left(\frac{W}{W_{\mathcal{P}}} - \frac{c_{p,\mathcal{P}}}{c_{p,m}}\right)\frac{\mathrm{d}Y_{\mathcal{P}}}{\mathrm{d}t}$$
$$+ \frac{q}{c_{p,m}T}\frac{\mathrm{d}Y_{\mathcal{P}}}{\mathrm{d}t}, \tag{4}$$

the right-hand side being the thermicity. The terms related to variation of the heat capacities and molar masses are represented in magenta, which are not present in the original three-step model. The consumption rates for the different species are

$$r_I = k_I' k_I (\rho Y_{\mathcal{F}}) \exp(-E_I/R_u T)$$
$$r_B = k_B' k_B (\rho Y_{\mathcal{F}})(\rho Y_{\mathcal{Y}})/W_{\mathcal{F}} \exp(-E_B/R_u T) \tag{5}$$
$$r_T = k_T' k_C (\rho Y_{\mathcal{Y}})$$

The corresponding pre-exponential factors for the initiation, branching and termination are $k_I = k_C \exp(E_I/R_u T_I)$, $k_B = k_C \exp(E_B/R_u T_B)$ and $k_T = k_C$, respectively. E_I/R_u and E_B/R_u are the initiation and branching activation temperatures, and T_I and T_B are the crossover temperatures at which the chain-initiation and branching rates become equal to the chain-termination rate. k_I', k_T', and k_B' are calibration coefficients, in green in Eq. 5.

The parameters are: $k_C = 2 \times 10^7\,\mathrm{s}^{-1}$, $E_I/R_u = 25\,000\,\mathrm{K}$, $E_B/R_u = 8500\,\mathrm{K}$, $T_I = 8500\,\mathrm{K}$, $T_B = 1350\,\mathrm{K}$ (from [9] after a calibration against constant volume combustion induction times). From Thompson [18], the CJ detonation velocity can be found to be

$$M_{\mathrm{CJ}} = \left[\mathcal{H} + \frac{(\gamma_{\mathcal{P}} - 1)(\gamma_{\mathcal{F}} + \gamma_{\mathcal{P}})}{2\gamma_{\mathcal{F}}(\gamma_{\mathcal{F}} - 1)}\right]^{1/2} + \left[\mathcal{H} + \frac{(\gamma_{\mathcal{P}} - \gamma_{\mathcal{F}})(\gamma_{\mathcal{P}} + 1)}{2\gamma_{\mathcal{F}}(\gamma_{\mathcal{F}} - 1)}\right]^{1/2}, \mathcal{H} = \frac{(\gamma_{\mathcal{P}} - 1)(\gamma_{\mathcal{P}} + 1)q}{2\gamma_{\mathcal{F}}R_{\mathcal{F}}T_0} \tag{6}$$

3   Numerical results

3.1   Results from the ZND model

The ZND reference profiles have been obtained from the SD-Toolbox [19]. The heat capacity and the molecular weight are related through the Meyer relation $\mathcal{R}_u/W_k = \frac{\gamma_k - 1}{\gamma_k}c_{p,k}$. The molecular weights

were determined at first, $W_{\mathcal{F}} = 12\,\text{g/mol}$, $W_{\mathcal{P}} = 14.4\,\text{g/mol}$ at the von Neumann (vN) and CJ states, respectively. The latter is different from that of the water vapor, due to dissociation at the high temperatures near stochiometry. This enabled to obtain temperatures that were close to the initial and end states of the ZND profile. Then, the isentropic coefficients were determined. Low values are indeed known to enhance cell irregularity through cell bifurcation [20, 21] and potential hot spots. The isentropic coefficient for $\mathcal{F}$ was determined in order to match as much as possible the temperature at the vN state. Then, $\gamma_{\mathcal{P}}$ was taken from the results of the SD-Toolbox. Then the heat of reaction is deduced from Eq. 6. All the thermodynamic parameters for the intermediate species $\mathcal{Y}$ were taken equal to that of the $\mathcal{F}$ species. Another approach is to calculate the heat of reaction q from the equilibrium detonation velocity D_{CJ} after supplementing Eq. 6 with the exact expression Eq. (72) for the equilibrium $\gamma_{\mathcal{P}}$ derived in [22].

In the first set of experiments (configuration 1), $k'_I = k'_B = k'_T = 1.0$. In the second set of experiments (configuration 2), $k'_I = 1$, $k'_B = 1.25$, $k'_T = 3.0$.
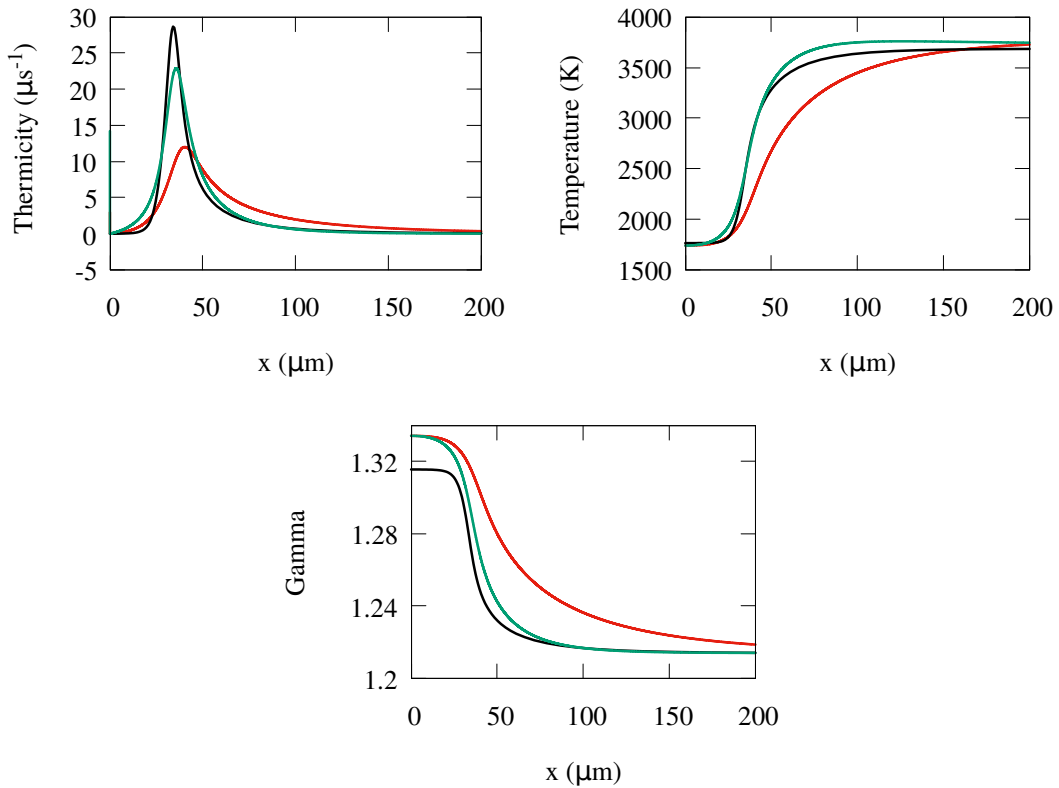
Figure 1: Comparaison between the thermicities (top left), temperatures (top right) and polytropic coefficient (bottom). Reference in black, configuration 1 in red, and configuration 2 in green.

From Fig. 1, the end state for the temperatures is almost the same for both configurations. However, the main difference was that thermicity was much better captured in configuration 2 with a rather slight modification of the pre-exponential factors. This also impacted the rate at which the other variables reached the end states. This also means that the χ parameter which measures the relative time scales of induction and heat deposition, is also better recovered. We recall $\chi = \frac{T_{\text{vN}}}{\tau_{\text{ind}}} \cdot \frac{\partial \tau_{\text{ind}}}{\partial T} \cdot \frac{\Delta_{\text{ind}}}{\Delta_{\text{reac}}}$, $\Delta_{\text{reac}} = u_{\text{CJ}}/\dot{\sigma}_{\text{max}}$. Again, this parameter has been used as a measure of the detonation cell regularity [23, 24].

3.2 Results from 2-D simulations

From the original parameters [9] (all molecular weights equal to $12\,\mathrm{g/mol}$, and constant isentropic coefficient equal to 1.33), first simulations have shown that the critical height for the transmission and propagation of the detonation was about $22\,\mathrm{mm}$, that is much greater from the experimental value of $6\,\mathrm{mm}$.

First computations, not shown here, have highlighted that the critical height for propagation was different from that of transmission and propagation. Progressive decrease of the reactive height has shown that the critical height for the detonation propagation was less than $15\,\mathrm{mm}$. This is reminiscent from the work of Murray and Lee [25], that showed that the rate of expansion imposed on the detonation wave was important for the determination of the critical height. Figure 2 shows numerical soot foil for the transmission and extinction of the detonation wave in a 15 mm height reactive mixture, for the initial parameters. The red dotted line delineates the reactive mixture from the inert one.
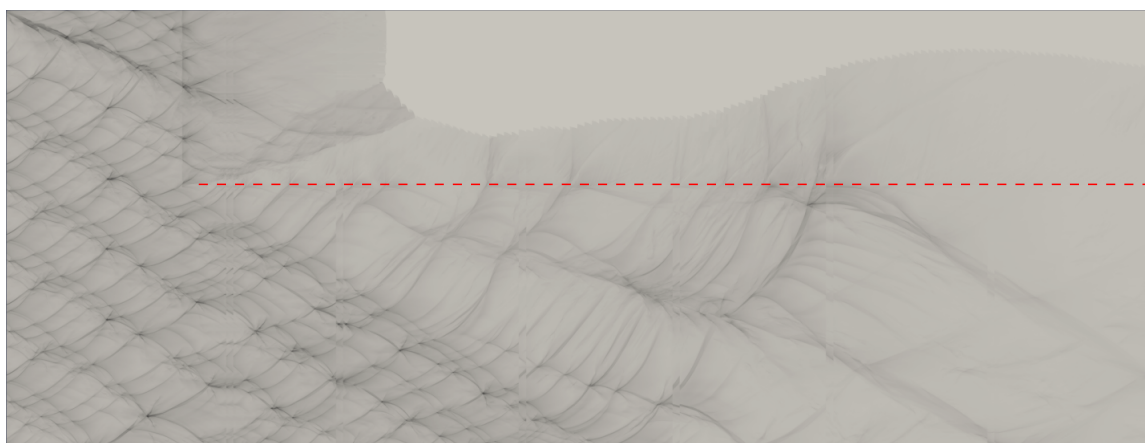
Figure 2: Numerical soot foil for the transmission and extinction of detonation wave in a $15\,\mathrm{mm}$ height reactive mixture. The total length is $65.24\,\mathrm{mm}$.

Hence, the reactive height is taken to be $15\,\mathrm{mm}$ in the following study. The resolution was 10 pts per $\Delta_{\mathrm{ind}} \approx 34\,\mu\mathrm{m}$. As for the initial configuration, $L_x \times L_y = 10\,\mathrm{mm} \times 25\,\mathrm{mm}$ and as for the two other configurations, $L_x \times L_y = 6\,\mathrm{mm} \times 26\,\mathrm{mm}$. We use 24 processors in the x direction and 30 in the y direction, with a typical mesh size of 13.5 million computational cells.

Fig. 3 shows the three different configurations. The left figure shows the extinction of the detonation with the original parameters. The middle figure shows a re-initiation process with the calibration of the thermodynamic parameters. The right figure shows that a steady propagation detonation with the calibration of the thermodynamic and kinetics calibrations.

3 Discussions

The initial three-step model has been at first modified in order to take into account thermodynamic changes of the products (molecular weight and γ). Then, a second modification has been made to the values of the pre-exponential factors in order to recover the thermicity profile of the ideal ZND model from detailed chemistry. To some degree, matching the thermicity profile, the calibration has also relied on targeting the γ and the χ parameters, which have been used to qualify the degree of irregularity of the detonation cellular structure. Preliminary 2-D results have shown that these two successive modifications enabled to come closer to the reference critical height, determined from detailed chemistry.
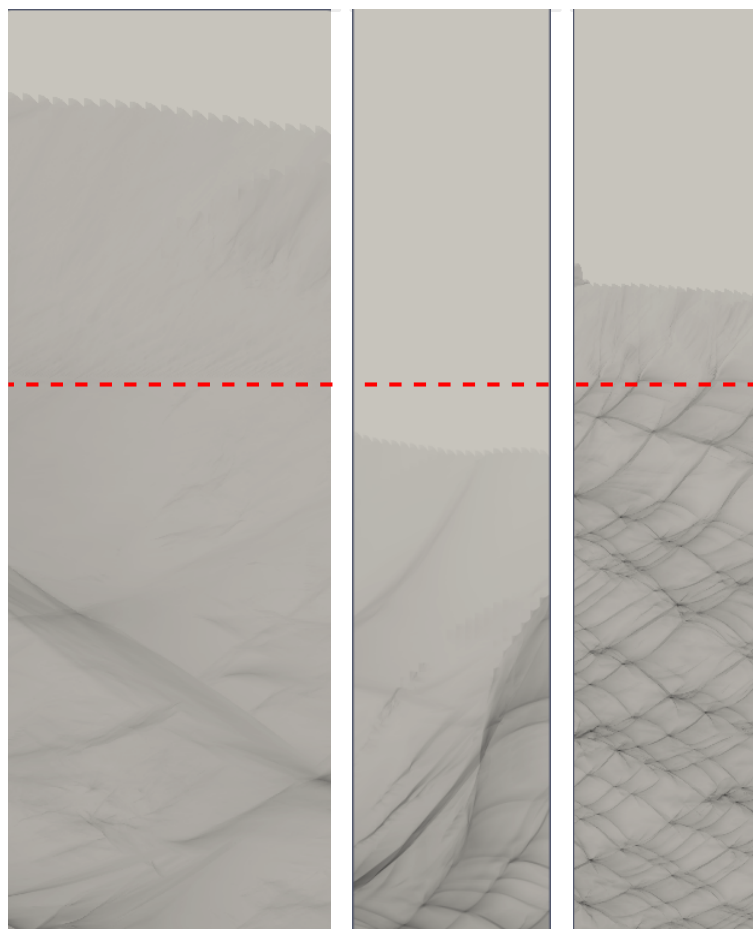
Figure 3: Comparaison between the 2-D simulations with three different chemical model parameters. Left: original [9], $56.87\,\text{mm}$-$65.24\,\text{mm}$. Middle: thermodynamic parameters calibrated (configuration 1), $132.583\,\text{mm}$-$137.625\,\text{mm}$. Right: thermodymamics and kinetics calibrated (configuration 2), $90.324\,\text{mm}$-$95.356\,\text{mm}$. The reactive height is $15\,\text{mm}$.

The results above are promising, but further computations should assess to which extent this modeling approach can reproduce the critical height determined from detailed chemistry. A more general goal should be to widen its thermodynamic and spatial representativeness.

Acknowledgements

References

[1] Lee, J.H.S. (2008) The detonation phenomenon. Cambridge University Press.

[2] Shepherd, J.E., Kasahara, J. (2017) Analytical models for the thrust of a rotating detonation engine. GALCIT Report FM2017.001

[3] W. Rudy, M. Kuznetsov, R. Porowski, A. Teodorczyk, J. Grune, K. Sempert (2013). Critical conditions of hydrogen-air detonation in partially confined geometry. Proc. Combust. Inst. 34:1965–1972.

[4] Short, M., Quirk, J. J. (2018). High explosive detonation–confiner interactions. Annu. Rev. Fluid Mech. 50:215-242.

[5] Reynaud, M., Virot, F., Chinnayya, A. (2017). A computational study of the interaction of gaseous detonations with a compressible layer. Phys. Fluids 29(5):056101.

[6] Reynaud, M., Taileb, S., Chinnayya, A. (2020). Computation of the mean hydrodynamic structure of gaseous detonations with losses. Shock Waves 30(6):645-669.

[7] Mi, X., Higgins, A., Kiyanda, C., Ng, H., Nikiforakis, N. (2018). Effect of spatial inhomogeneities on detonation propagation with yielding confinement. Shock Waves 28:993–1009.

[8] Houim, R.W., Fievisohn, R.T. (2017). The influence of acoustic impedance on gaseous layered detonations bounded by an inert gas. Combust. Flame 179:185–198.

[9] Taileb, S., Melguizo-Gavilanes, J., Chinnayya, A. (2020). Influence of the chemical modeling on the quenching limits of gaseous detonation waves confined by an inert layer. Combust. Flame 218:247-259.

[10] Shigeoka, S., Matsuo, A. Kawasaki, A., Kasahara J., Matsuoka, K. (2019). The Numerical Investigation of Hydrogen Detonation Propagating in Semi-confined Layers, ICDERS 2019, Beijing, China, Proceedings of the 27th International Colloquium on the Dynamics of Explosions and Reactive Systems, Paper 138, 2019.

[11] Lu, X., Kaplan, C.R., Oran, E.S. (2021). A chemical-diffusive model for simulating detonative combustion with constrained detonation cell sizes, Combust. Flame 230:111417

[12] Houim, R.W., Taylor, B.D. (2019). Detonation initiation from shock and material interface interactions in hydrogen-air mixtures, Proc. Combust. Inst. 37(3):3513-3520

[13] Veiga Lopez F., Melguizo-Gavilanes, J., Chinnayya A. (2022), A methodology to develop simplified kinetic schemes for detonation simulation, submitted to ICDERS 2022, Naples, Italy

[14] Dold, J.W., Kapila, A.K. (1991). Comparison between shock initiations of detonation using thermally-sensitive and chain-branching chemical models. Combust. Flame 85(1-2):185-194.

[15] Sharpe, G.J., Maflahi, N. (2006). Homogeneous explosion and shock initiation for a three-step chain-branching reaction model, J. Fluid Mech. 566:163–194.

[16] Melguizo-Gavilanes, J., Bauwens, L. (2013). A comparison between constant volume induction times and results from spatially resolved simulation of ignition behind reflected shocks: implications for shock tube experiments. Shock Waves 23:221–231.

[17] Higgins, A. (2012). Steady one-dimensional detonations. In Shock Waves Science and Technology Library, Vol. 6, pp. 33-105. Springer, Berlin, Heidelberg.

[18] Thompson, P.A. (1972) Compressible fluid dynamics. Mc-Graw Hill.

[19] Browne, S., Ziegler, J., Shepherd, J.E. (2008) GALCIT report FM2006, Vol. 6, pp. 90.

[20] Sow, A., Lau-Chapdelaine, S.M., Radulescu, M.I. (2021). The effect of the polytropic index γ on the structure of gaseous detonations. Proc. Combust. Inst 38(3):3633-3640.

[21] Taileb, S., Melguizo-Gavilanes, J.,Chinnayya, A. (2021). The influence of the equation of state on the cellular structure of gaseous detonations. Phys. Fluids 33(3):036105.

[22] Vidal, P., Zitoun, R. (2020). A Velocity-Entropy Invariance theorem for the Chapman-Jouguet detonation. doi: https://arxiv.org/abs/2006.12533

[23] Radulescu, M.I. (2003). The propagation and failure mechanism of gaseous detonations: experiments in porous-walled tubes, Ph.D. thesis, McGill University Libraries, 2003.

[24] Ng, H.D., Zhang, F. (2012). Detonation instability. In Shock Waves Science and Technology Library, Vol. 6 (pp. 107-212). Springer, Berlin, Heidelberg.

[25] Murray, S.B., Lee, J.H.S. (1986). The influence of physical boundaries on gaseous detonation waves, Progress in Astronautics and Aeronautics 106:329-355